J Biomol NMR (2012) 54:115–121
DOI 10.1007/s10858-012-9654-1

NMR STRUCTURE NOTE

NMR structure note: solution structure of Ca^{2+} binding domain 2B of the third isoform of the Na^+/Ca^{2+} exchanger

Vincent Breukels · Wouter G. Touw · Geerten W. Vuister

Received: 16 May 2012 / Accepted: 30 June 2012 / Published online: 18 July 2012

Abbreviations

CBD2	Ca^{2+} binding domain 2
HEPES	4-(2-hydroxyethyl)-1-piperazineethanesulfonic acid
K_D	Macroscopic dissociation constant
ITC	Isothermal titration calorimetry
NCX3	Na^+/Ca^{2+} exchanger isoform 3
NOE	Nuclear Overhauser effect
OD_{600}	Optical density at 600 nm
RDC	Residual dipolar coupling
r.m.s.	Root mean square
r.m.s.d.	Root mean square deviation
SDS-PAGE	Sodium dodecyl sulfate polyacrylamide gel electrophoresis

Electronic supplementary material The online version of this article (doi:10.1007/s10858-012-9654-1) contains supplementary material, which is available to authorized users.

V. Breukels · W. G. Touw
Institute for Molecules and Materials, Radboud University Nijmegen, Geert Grooteplein 26-28, 6525 GA Nijmegen, The Netherlands

Present Address:
V. Breukels
Department of Radiology, Radboud University Nijmegen Medical Centre, Geert Grooteplein 10, 6526 GA Nijmegen, The Netherlands

G. W. Vuister (✉)
Department of Biochemistry, University of Leicester, Henry Wellcome Building, Lancaster Road, Leicester LE1 9HN, UK
e-mail: gv29@le.ac.uk

Biological context

The Na^+/Ca^{2+} exchanger (NCX) is an omnipresent plasma membrane protein that catalyzes the removal of intracellular Ca^{2+} for the uptake of Na^+ [see for review (Lytton 2007)]. Mammals express three isoforms, denoted as NCX1, NCX2, or NCX3, of which isoforms 1 and 3 also display alternative splicing. The exchanger is activated by allosteric Ca^{2+} binding to Ca^{2+} binding domains 1 and 2 (CBD1 and CBD2) located in the large cytosolic loop between transmembrane helix 5 and 6. CBD1 binds four Ca^{2+} ions, irrespective of the isoform and is considered the primary Ca^{2+} sensor. The number of Ca^{2+} ions that bind to CBD2 depends on the isoform and splice variant. It is hypothesized that the number of binding sites determines the ability of the exchanger to overcome the Na^+ dependent inactivation (Hilge et al. 2009) and that Mg^{2+} binding plays a modulating role (Boyman et al. 2009; Breukels et al. 2011).

NCX1 is thus far the best-studied isoform and solution or X-ray structures of NCX1 CBD1 and CBD2 have been determined (Besserer et al. 2007; Hilge et al. 2006, 2009; Nicoll et al. 2006). CBD1 and CBD2 display an immunoglobulin like fold comprised of seven β-strands. The Ca^{2+} binding pocket is formed by the loops connecting the β-strands. CBD2 of NCX1 is further characterized by an α-helix in the large, otherwise unstructured FG-loop opposite to the Ca^{2+} binding pocket as well as by two β-bulges disrupting the hydrogen bonding pattern of strands βA and βG. In the intact exchanger a very short linker connects CBD1 and CBD2 and the two domains adopt an elongated orientation with the Ca^{2+}-binding pocket of CBD1 close to the FG-loop of CBD2 (Salinas et al. 2011; Wu et al. 2011). Ca^{2+} binding induces changes in the relative domain orientation, possibly through interaction between CBD1 and the FG-loop of CBD2.

The third mammalian isoform of the NCX (NCX3) is mainly found in brain and skeletal muscle (Nicoll et al. 1996). NCX3 is subject to alternative splicing that involves exons A, B and C. The alternative splicing region affects CBD2 and alters the number of Ca^{2+} binding sites. NCX3-CBD2-AC binds two Ca^{2+}, whereas NCX3-CBD2-B and NCX3-CBD2-BC bind three Ca^{2+} ions (Hilge et al. 2009). Here, we present the solution structure of NCX3-CBD2-B.

Methods and results

Protein expression and purification

The CBD2-B construct was derived from *mus musculus* NCX3 (accession code: Q7TS90) and cloned into a pET23b vector as previously described (Hilge et al. 2009). Uniformly ^{15}N and $^{15}N/^{13}C$ labelled protein was obtained by growing *E. coli* BL21(DE3) in 800 mL of minimal M9 medium in the presence of ^{15}N ammonium chloride and ^{13}C-glucose (Cambridge Isotope Laboratories Inc.) at 37°C and induction by 1 mM isopropyl-β-D-thio-galactoside for ~4 h at an OD_{600} of 1.0. Purification was facilitated by N-terminal His tag and anion-exchange chromatography (MonoQ, Amersham-Pharmacia). Purity of all samples was >95 % as judged by SDS-PAGE and ^{15}N-HSQC spectra. The samples were concentrated using a 10 kDa molecular weight cut off Vivaspin 6 (GE Healthcare) and contained ~0.5 mM protein in 20 mM HEPES (pH 7.0), 20 mM β-mercaptoethanol, 10 mM $CaCl_2$ buffer prepared in 95 %/5 % H_2O/D_2O with 0.03 % NaN_3 as preservative. The alignment medium used for Residual Dipolar Couping (RDC) measurements contained Pf1 phage (ASLA Biotech) with an optimized concentration of 8 mg/mL and 0.3 mM protein in an otherwise identical buffer. Under these conditions a quadrupolar splitting of 3.4 Hz was observed in the ^2H NMR spectrum. All chemicals were obtained from Sigma Aldrich unless stated otherwise.

Resonance assignments

NMR spectra were acquired at 306 K on Varian Inova 600 and 800 MHz spectrometers equipped with a standard triple resonance probe and a cold probe, respectively. Backbone resonance assignment was obtained using the following experiments: ^{15}N-HSQC, HNCO, HNCACB, CBCA(CO)NH and HN(CA)HA. The side chain chemical shifts were obtained using the experiments: HBHA(CO)NH, C(CO)NH, H(C)CH-TOCSY, (H)CCH-TOCSY. Side-chain assignments were improved by analyzing NOE resonances predicted from preliminary structures calculated using distance, dihedral and RDC restraints. Aromatic side chain assignments were obtained from the ^{13}C-NOESY-HSQC (aromatic). All spectra were processed with the NMRPipe program (Delaglio et al. 1995) and analyzed with CCPN Analysis (Vranken et al. 2005).

Protein resonance assignments were achieved for 83.1 % of all backbone atoms and 77.4 % for all H side-chain assignments. Backbone and side-chain resonance assignments were missing for residues 605–610 in the EF-loop and residues 665–669 near the C-terminus. These residues are near the Ca^{2+} binding pocket and are in chemical exchange between the apo- and Ca^{2+}-form bound form. Possibly, the missing resonances are exchange line broadened beyond detection (cf. Discussion). The chemical shift assignments were deposited in the BMRB accession code 18464.

Structure determination

Distance restraints for structure calculation were derived from ^{13}C-NOESY-HSQC (aliphatic and aromatic) and ^{15}N-NOESY-HSQC spectra recorded with 80 ms NOE-mixing time. For structure determination the NOESY cross peaks were automatically picked and integrated by CCPN Analysis and manually checked for artefacts and genuinely missed peaks. The input data for CYANA3.0 (Güntert 2009) consisted of the chemical shifts obtained from the resonance assignment, the unassigned peak positions and volumes of the NOESY spectra, 186 backbone dihedral restraints based on the chemical shift information from the program TALOS+ (Shen et al. 2009) and 81 ^1H-^{15}N RDCs. The NOESY peak lists were automatically assigned during seven cycles of automated assignment and structure calculation. In each cycle one hundred structures were generated and energy minimized using 15,000 steps of simulated annealing. The NOE calibration parameters were automatically determined in the first cycle. In the 7th cycle 4,983 of the 7,431 NOESY peaks were assigned. The 20 lowest energy conformers were subsequently subjected to a final round of refinement in explicit solvent using the YASARA force field and the YASARA software (www.yasara.org), in which RDC restraints were not included, as the current version of YASARA cannot yet accommodate these. Overall structural statistics of the final water-refined structure are shown in Table 1. The Ca^{2+} ions were not modelled in the structure because of missing resonance assignments in the Ca^{2+} binding pocket. The coordinates of NCX3-CBD2-B were deposited in the PDB under accession code 2lt9.

The solution structure of NCX3-CBD2-B displays the Calx-β fold (Fig. 1A). The core of NCX3-CBD2-B is formed by seven β-strands (labelled βA to βF). As in the previously reported structures of CBD2, two β-bulges in NCX3-CBD2-B disrupt the hydrogen-bonding pattern of strands βA and βG (labelled βA/βA′ and βG/βG′). The

hydrogen bonding pattern is the result of the structure calculation and subsequent water refinement without the use of explicit hydrogen bond restraints. The strands form a β-sandwich comprised of two β-sheets consisting of strands GABE and strands DCFG′A′. Although the first part of the FG-loop is largely unstructured, an α-helix is present in the second part of the FG-loop (residues 638–650, vide infra). In total, NCX3-CBD2-B is nine residues shorter compared to NCX1-CBD2-AD and outside the FG-loop the two proteins display a sequence identity of ~76 % (Fig. 1C). The N-terminal signal sequence of NCX1 is cleaved off during maturation (Durkin et al. 1991). In contrast, a similar cleavage has not been biochemically verified for NCX3 to date. Therefore, equivalent residues in both proteins have a numbering offset of 27 in the structure reported here. A structural alignment of NCX3-CBD2-B with NCX1-CBD2-AD (Fig. 1B) shows the two proteins to be structurally very similar, resulting in a heavy atom backbone r.m.s.d. of 1.11 ± 0.04 Å for the β-sandwich residues.

Residual dipolar couplings

116 ^{1}H-^{15}N RDCs were obtained from in-phase/anti-phase ^{15}N-HSQC experiments, by comparing the peak positions of the up-field and down-field components measured in isotropic solution and the dilute liquid crystalline phase. Eighty-one RDCs were measured for residues in the β-sandwich, the α-helix, and the very short stretch connecting the helix to βG (Fig. 2A). This subset, referred to as the 'standard RDC set', was used to restrain the orientation of amide bond vectors relative to a common alignment frame during the CYANA structure calculation protocol. A detailed analysis with respect to the influence of the RDC restraints on the orientation of the α-helix is given in the Supplementary Materials. The correlation between observed and predicted RDCs is shown in Fig. 2B for the lowest-energy conformer after refinement in explicit water. RDCs and alignment tensors were fitted to the structure in CYANA3.0 using singular value decomposition. The Q factor (Cornilescu et al. 1998) was 15 ± 1 % after the CYANA calculations, which increased to 35 ± 1 % after refinement in water that excluded these RDCs.

Backbone dynamics

T_1, $T_{1\rho}$ and ^{1}H-^{15}N steady state NOE experiments were recorded at 18.8 T in an interleaved fashion. The recorded time intervals for the T_1 and $T_{1\rho}$ were 16, 256, 384, 512, 768 and 1,024 ms and 16, 32, 48, 64, 96 and 128 ms, respectively. The time delay between the saturated and unsaturated parts in the NOE experiments was 13 s. The relaxation rates were determined as previously described (Breukels and Vuister 2010) and amide backbone dynamics were derived according to the model-free analysis formulated by Lipari and Szabo implemented in the program Tensor2 (Dosset et al. 2000).

The rotational diffusion anisotropy of NCX3-CBD2-B was best described by an axial symmetric diffusion tensor, characterized by a $D_{\parallel}/D_{\perp}$ ratio of 1.68 ± 0.03 and an overall tumbling correlation time $\tau_{av,aniso}$ of 11.6 ± 0.14 ns. The generalized order parameter S^2 is plotted as a function of residue number in Fig. 2C. The mean S^2 values are 0.94, 0.80, and 0.55 in the β-sandwich, α-helix, and the first part the FG-loop before the helix, respectively.

Table 1 Structural statistics of the 20 lowest energy structures of NC3-CBD2-B after water-refinement in YASARA

Number of NOE restraints	
2,901	Total NOE restraints
1,333	Short range (|i − j| <= 1)
279	Medium range (1 < |i −j| < 5)
1,289	Long range (|i −j| > 5)
Distance restraints violations	
0	In six or more structures >0.2 Å
0	In six or more structures >0.3 Å
0.004 ± 0.001	r.m.s
TALOS+ derived dihedral restraints	
93	φ
93	ψ
Dihedral violations	
1	In six or more structures >5°
1.71 ± 0.05	r.m.s
Number of RDC restraints	
81	^{1}H-^{15}N
RDC violations (after refinement without RDCs)	
2	In six or more structures >5 Hz
1.74 ± 0.09	r.m.s
34.5 ± 1.5	Q-factor
Ramachandran plot (%)	
80.9	Residues in the most favored region
15.6	Residues in the additionally allowed region
2.2	Residues in the generously allowed region
1.3	Residues in the disallowed region
Cing ROG scores	
24.3/32.4/43.3	ROG (%)
r.m.s.d. to the average coordinates for β-sandwich	*Residues:531–542, 546–556, 561–570, 581–589, 594–602, 612–624, 638–665*
0.37 ± 0.07	Backbone heavy atom
0.75 ± 0.07	All heavy atom

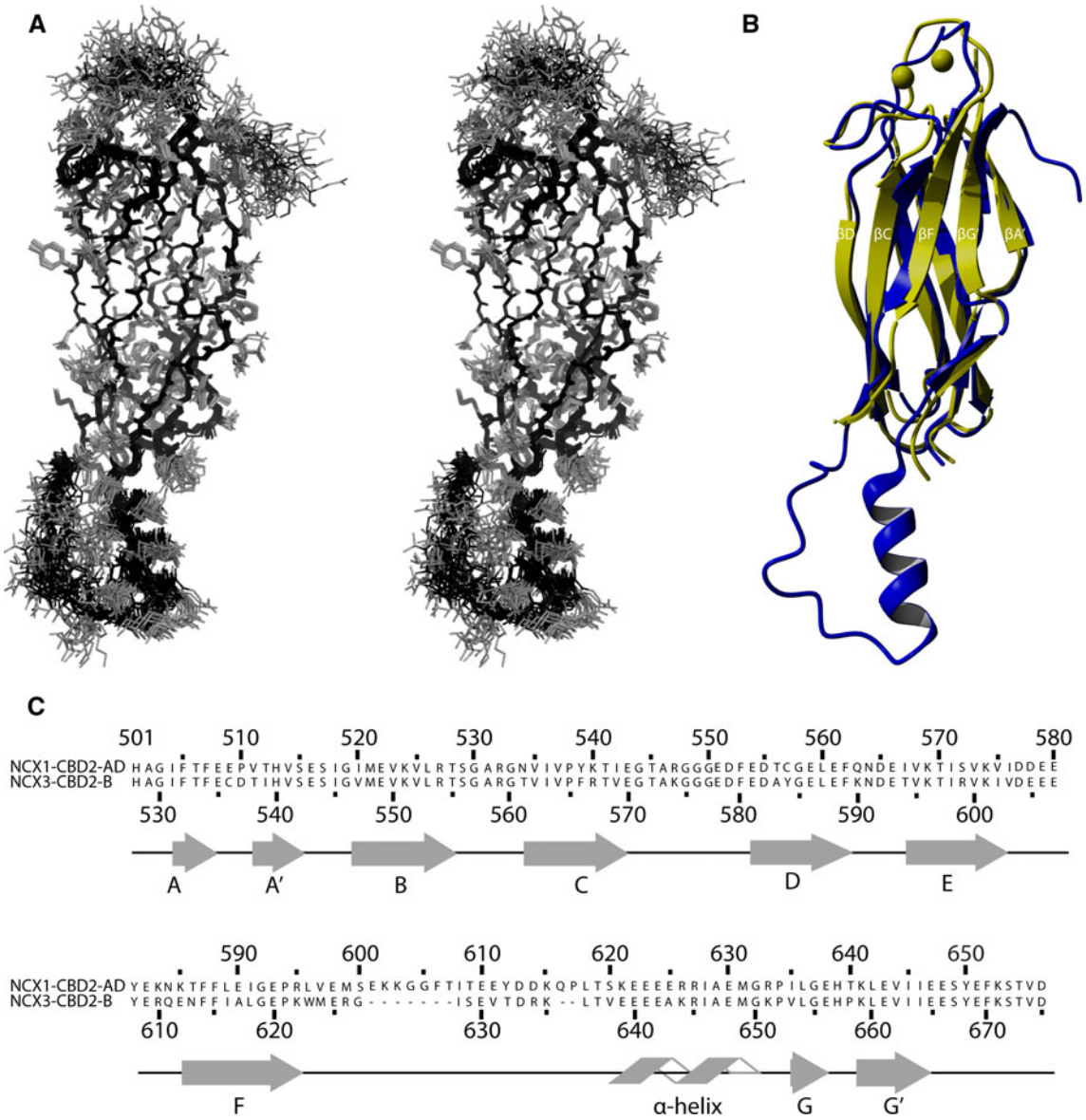

Fig. 1 Solution structure of NCX3-CBD2-B (PDB: 2lt9). **A** Stereo view of the structural ensemble. Backbone and side chains are represented as *black* and *grey sticks*, respectively. **B** Structural alignment of the lowest-energy conformer (*blue*) and NCX1-CBD2-AD (2QVM, *yellow*). Ca^{2+} ions are only shown for the crystal structure because crucial resonances were missing in the Ca^{2+} binding pocket of NCX3-CBD2-B. The alignment was based on residues of the β-sandwich. Residues 571–575 in NCX3-CBD2-B were omitted from (**A**) and (**B**) for clarity. Strand labels are indicated. Figures created with Pymol (www.pymol.org) and YASARA (www.yasara.org). **C** Sequence alignment of canine NCX1-CBD2-AD and mouse NCX3-CBD2-B, with the residue numbering indicated above and below, respectively. The β-strands and the α-helix are indicated in the topology diagram below the alignment

We observed internal motion in the FG-loop characterized by an internal correlation time τ_i of 1.0 ± 0.5 ns. An extra apparent conformational exchange contribution of 1.6 ± 1.5 s^{-1} was sufficient for the helix but not the remainder of the FG loop to explain the measured relaxation data (Suppl. Fig. S1 A,C and E). The dynamics of the first part of the FG loop could only be accurately described by a modified Lipari-Szabo model that includes both motions on a time-scale much faster than the overall protein rotation, and slower internal dynamics with a correlation time comparable to $\tau_{av,aniso}$.

Water refinement and structure validation

The water refinement of the protein structure was performed in YASARA. Unfortunately, YASARA only restrains inter-atomic distances and dihedral angles but not the orientation of amide bond vectors. In contrast, Xplor-

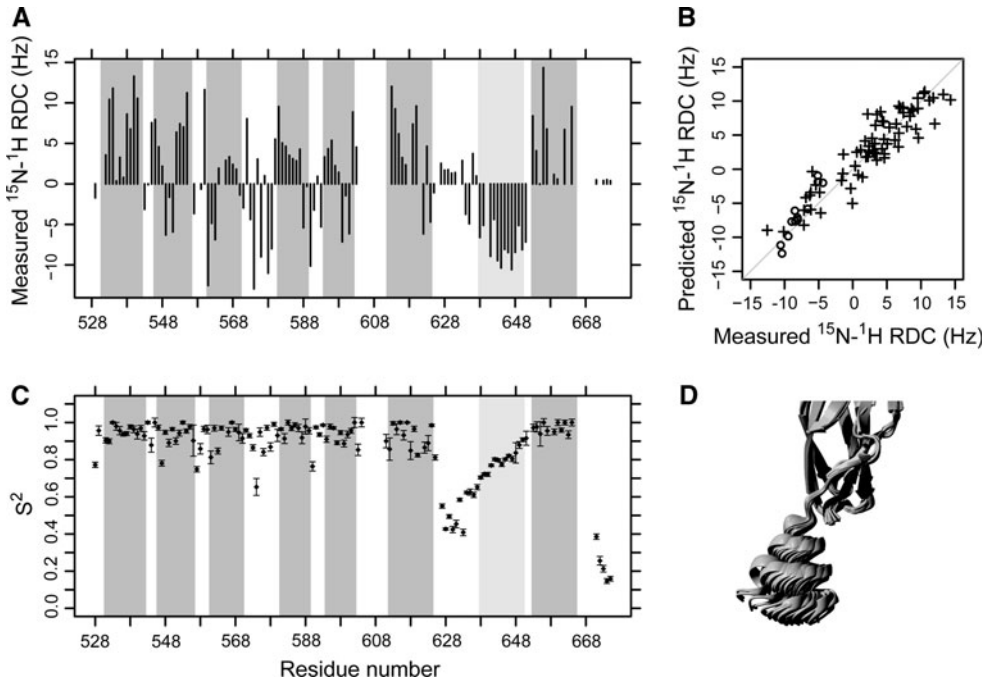

Fig. 2 **A** Measured ^{1}H-^{15}N RDC values as function of residue number. The estimated uncertainty is 0.8 Hz. Secondary structure elements are represented by *dark* (*β*-strands) and *light* (α-helix) *grey rectangles*. **B** Correlation between measured and back-calculated RDCs using the lowest-energy conformer of the structural ensemble. *Circles* indicate α-helix residues, crosses indicate residues in *β* strands and residues connecting the α-helix to *β*G. The *grey line* represents a perfect correlation. **C** Generalized ^{15}N order parameter, S^2, as function of residue number. **D** Comparison of α-helix orientations in eight separate structure determinations calculated with different sets of α-helix RDC restraints, but using otherwise identical RDC restraints for all other residues. All structures were aligned using backbone heavy-atoms in the *β*-sandwich

NIH (version 2.27) can use RDC potentials during the simulated annealing protocol. In our hands, the standard Xplor-NIH water-refinement protocol over-refined the RDCs at the cost of very high dihedral and Ramachandran energies (cf. Supplementary Materials). Hence, the best structures in terms of fit with the experimental data and common criteria for structural quality were obtained when the CYANA calculations were followed by a refinement protocol in explicit water using the YASARA force-field. The reported structures were validated using the iCING web server (http://nmr.cmbi.ru.nl/icing/). The iCING web server employs several different validation programs, such as PROCHECK_NMR, Aqua and Whatif, and assigns a per residue ROG-score (Red, Orange and Green) for problematic, reasonable and good residues, respectively. Overall validation statistics are reported in Table 1.

The orientation of the helix with respect to the *β*-sandwich differs from the orientation observed for NCX1-CBD2-AD. To validate our present results, we performed several additional structure calculations using identical distance and dihedral restraints, but with less or no α-helical RDC restraints (cf. Supplementary Materials). A comparable α-helix orientation was obtained, even when all α-helix RDC restraints were excluded from the calculations. The analysis further showed that the helix samples a number of conformations that fit similarly well to the observed RDC restraints (Fig. 2D). The relaxation data also support the existence of multiple conformations, because conformational exchange contributions to the motion of the NH-bond vectors of residues in the helix were observed.

Discussion and conclusions

In this study we present the first structure of the second Ca^{2+} binding domain of the third NCX isoform. NCX3-CBD2-B adopts the Calx-*β* fold comprised of seven *β*-strands forming a *β*-sandwich. In the CBDs of NCX1 the loops connecting the *β*-strands *β*A-*β*B, *β*C-*β*D and *β*E-*β*F form the Ca^{2+} binding pocket (Hilge et al. 2006; Nicoll et al. 2006) and a similar arrangement is observed for NCX3-CBD2-B. Our structure shows that the *β*-bulges are conserved between the various NCX isoforms suggesting a potential, albeit yet unknown, role in NCX functioning.

For NCX3-CBD2-B we were unable to find resonances for residues in the EF-loop, as well as in the C-tail. This lack of resonances has also been observed for residues in the EF-loop of NCX1-CBD2-BD, a CBD variant unable to bind Ca^{2+} (Hilge et al. 2009). The lack of resonances possibly originates from unfavourable dynamics of the

Ca^{2+} binding loops. In a previous study we showed that the Ca^{2+}-binding loops in the apo form of NCX1-CBD2-AD are more flexible than in the Ca^{2+} bound form (Breukels and Vuister 2010). As a result, the apo form has a lower overall correlation time ($\tau_{av,aniso}$ ~11.4 ns) and a less anisotropic diffusion tensor ($D_{\|}/D_{\perp}$ ~1.4) than the Ca^{2+} bound form ($\tau_{av,aniso}$ ~13.1 ns and $D_{\|}/D_{\perp}$ ~2.1). In comparison, the overall dynamics of NCX3-CBD2-B ($\tau_{av,aniso}$ ~11.6 ns and $D_{\|}/D_{\perp}$ ~1.7) is more similar to the apo form of NCX1-CBD2-AD compared to the Ca^{2+}-bound form. Furthermore, isothermal titration calorimetry (ITC) data of NCX3-CBD2-B shows that the three Ca^{2+} ions have macroscopic dissociation constants (K_D) of 3.9, 8.3 and 19 μM (Hilge et al. 2009), which is almost ten times higher than the Ca^{2+} affinity of NCX1-CBD2-AD (K_D of 0.4 and 1.1 μM, (Breukels et al. 2011). The decreased affinity either originates from a lower k_{on} or higher k_{off} and the latter would result in increased chemical exchange effects. Based on the ^{15}N-relaxation data, we derive significant chemical exchange rates for residues in the CD Ca^{2+} binding loop (2–12.5 s^{-1}, Suppl. Fig. S1 E). This is indicative for conformational exchange of the CD-loop, possibly as a result of binding and release of Ca^{2+}. Therefore, the Ca^{2+} binding affinity together with the relaxation data strongly support the hypothesis that the resonances of residues in the EF-loop and C-tail are exchange line broadened beyond detection as a result of exchange between the apo and Ca^{2+} bound form, even at an excess of 10 mM $CaCl_2$.

The orientation of the α-helix in NCX1-CBD2-B differs from that observed in the NMR structure of NCX1-CBD2-AD, which might originate from lack of NCX1-CBD2-AD RDC data rather than genuine differences between the two isoforms. To test this hypothesis, we also measured the ^{1}H-^{15}N RDCs of NCX1-CBD2-AD (Suppl. Fig. S3 A). The data only agree with an α-helix oriented parallel to the β-sandwich, similar to the orientation in NCX3-CBD2-B (Suppl. Fig 3 B-E). It is possible that the alignment medium restricts the motion of the FG-loop and thereby imposes a restriction of the possible α-helix orientations. However, ^{15}N-relaxation measurements of NCX3-CBD2-B in Pf1 alignment medium show that the internal motion of the FG-loop is similar to FG-loop in the isotrope sample, although a reduction of chemical exchange terms is observed (Suppl. Fig S1).

In contrast to NCX, the FG-loop of the second Ca^{2+} binding domain of *Drosophila melanogaster* Na^{+}/Ca^{2+} exchanger (CALX-CBD2) is observed in its crystal structure (Wu et al. 2009). This FG-loop has two α-helices, one at the end of the βF-strand (H1) and one just before the βG-strand (H2). H2 adopts an orientation parallel to the long axis of the β-sandwich (Wu et al. 2009), very similar to orientation of the α-helix we report here for NCX3-CBD2-B. A X-ray study of CALX-CBD12 (Wu et al. 2011) showed that the two CBDs adopt an elongated orientation, which was also proposed for NCX-CBD12 (Salinas et al. 2011). In the CALX-CBD12 structure H2 is located at the CBD12 interface in close proximity to the Ca^{2+} binding sites of CBD1 and ITC and mutational analysis showed that several residues in H2 influence the Ca^{2+} binding of CBD1. We speculate that a similar domain interaction is present in NCX3, which likewise involves the α-helical region of CBD2.

A recent crystal structure of a E454K-NCX1-CBD12 (pdb: 3us9) construct shows that also in NCX1 the α-helical region is involved in the inter-domain interaction (Giladi et al. 2012). The α-helix in this structure is oriented parallel to the β-sandwich and fit our RDC data of NCX1-CBD2-AD well (Suppl. Fig. S3 F, G). Interestingly, the α-helix in E454K-NCX1-CBD12 spans residues 620 through 629 (NCX1 numbering), whereas it is four residues shorter in the NCX1-CBD2 NMR structure (residues 625 through 630, pdb: 2fwu). Likewise, the NCX3-CBD2-B α-helix is also shorter and we speculate that the increased length in E454K-NCX1-CBD12 is due to its interaction with CBD1. Finally, our ^{15}N-relaxation data and RDC analysis shows that in the NCX3-CBD2-B domain the α-helix adopts multiple conformations with respect to the β-sandwich. This could explain the difficulties of Giladi et al. in analyzing the SAXS data using a rigid body approach, as the FG-loop remains flexible even in the presence of CBD1.

In summary, we have determined the solution structure of NCX3-CBD2-B. The β-sandwich core of the protein is structurally very similar to previously reported NCX CBDs. The α-helix adopts an orientation that is primarily parallel to the β-sandwich, in line with recent studies that showed that this α-helix is part of the CBD12 interface, suggesting the NCX3-CBD2-B structure to represent a biologically relevant conformation.

Acknowledgments We thank Jurgen Doreleijers for assistance with Xplor-NIH and iCing, Gjalt van Rutten for support with using the HPC Cloud infrastructure at BitBrains. This work was supported by grants from the Netherlands Organization for Scientific Research (NWO): 700.55.443 and 700.57.101.

References

Besserer GM, Ottolia M, Nicoll DA, Chaptal V, Cascio D, Philipson KD, Abramson J (2007) The second Ca2+ -binding domain of the Na+ -Ca2+ exchanger is essential for regulation: crystal structures and mutational analysis. P Natl Acad Sci USA 104:18467–18472

Boyman L, Mikhasenko H, Hiller R, Khananshvili D (2009) Kinetic and equilibrium properties of regulatory calcium sensors of NCX1 protein. J Biol Chem 284(10):6185–6193

Breukels V, Vuister GW (2010) Binding of calcium is sensed structurally and dynamically throughout the second calcium-binding domain of the sodium/calcium exchanger. Proteins 78(8):1813–1824

Breukels V, Konijnenberg A, Nabuurs SM, Touw WG, Vuister GW (2011) The second Ca(2+)-binding domain of NCX1 binds Mg(2+) with high affinity. Biochemistry 50(41):8804–8812

Cornilescu G, Marquardt J, Ottiger M, Bax A (1998) Validation of protein structure from anisotropic carbonyl chemical shifts in a dilute liquid crystalline phase. J Am Chem Soc 120(27): 6836–6837

Delaglio F, Grzesiek S, Vuister GW, Zhu G, Pfeifer J, Bax A (1995) NMRPipe—a multidimensional spectral processing system based on UNIX pipes. J Biomol NMR 6:277–293

Dosset P, Hus JC, Blackledge M, Marion D (2000) Efficient analysis of macromolecular rotational diffusion from heteronuclear relaxation data. J Biomol NMR 16(1):23–28

Durkin JT, Ahrens DC, Pan YC, Reeves JP (1991) Purification and amino-terminal sequence of the bovine cardiac sodium-calcium exchanger: evidence for the presence of a signal sequence. Arch Biochem Biophys 290(2):369–375

Giladi M, Sasson Y, Fang X, Hiller R, Buki T, Wang Y-X, Hirsch JA, Khananshvili D (2012) A common Ca^{2+}-driven interdomain module governs eukaryotic NCX regulation. PLoS One 7(6): e39985

Güntert P (2009) Automated structure determination from NMR spectra. Eur Biophys J Biophy 38(2):129–143

Hilge M, Aelen J, Vuister GW (2006) Ca2+ regulation in the Na+/Ca2+ exchanger involves two markedly different Ca2+ sensors. Mol Cell 22(1):15–25

Hilge M, Aelen J, Foarce A, Perrakis A, Vuister GW (2009) Ca2+ regulation in the Na+/Ca2+ exchanger features a dual electrostatic switch mechanism. Proc Natl Acad Sci USA 106(34):14333–14338

Lytton J (2007) Na+/Ca2+ exchangers: three mammalian gene families control Ca2+ transport. Biochem J 406(3):365–382

Nicoll DA, Quednau BD, Qui ZY, Xia YR, Lusis AJ, Philipson KD (1996) Cloning of a third mammalian Na+ -Ca2+ exchanger, NCX3. J Biol Chem 271(40):24914–24921

Nicoll DA, Sawaya MR, Kwon S, Cascio D, Philipson KD, Abramson J (2006) The crystal structure of the primary Ca2+ sensor of the Na+/Ca2+ exchanger reveals a novel Ca2+ binding motif. J Biol Chem 281(31):21577–21581

Salinas RK, Bruschweiler-Li L, Johnson E, Bruschweiler R (2011) Ca2+-binding alters the inter-domain flexibility between the two cytoplasmic calcium-binding domains in the Na+/Ca2+ exchanger. J Biol Chem 286(37):32123–32131

Shen Y, Delaglio F, Cornilescu G, Bax A (2009) TALOS+ : a hybrid method for predicting protein backbone torsion angles from NMR chemical shifts. J Biomol NMR 44(4):213–223

Vranken WF, Boucher W, Stevens TJ, Fogh RH, Pajon A, Llinas P, Ulrich EL, Markley JL, Ionides J, Laue ED (2005) The CCPN data model for NMR spectroscopy: development of a software pipeline. Proteins 59(4):687–696

Wu M, Wang M, Nix J, Hryshko LV, Zheng L (2009) Crystal Structure of CBD2 from the drosophila Na(+)/Ca(2+) exchanger: diversity of Ca(2+) regulation and its alternative splicing modification. J Mol Biol 387(1):104–112

Wu M, Tong S, Gonzalez J, Jayaraman V, Spudich JL, Zheng L (2011) Structural basis of the Ca(2+) inhibitory mechanism of drosophila Na(+)/Ca(2+) exchanger CALX and its modification by alternative splicing. Structure 19(10):1509–1517